J Mol Med (2008) 86:291–302
DOI 10.1007/s00109-007-0274-2

ORIGINAL ARTICLE

Quantum dot-induced epigenetic and genotoxic changes in human breast cancer cells

Angela O. Choi · Shelley E. Brown · Moshe Szyf · Dusica Maysinger

Received: 16 February 2007 / Revised: 14 August 2007 / Accepted: 24 September 2007 / Published online: 27 October 2007

Abstract The staggering array of nanotechnological products, found in our environment and those applicable in medicine, has stimulated a growing interest in examining their long-term impact on genetic and epigenetic processes. We examined here the epigenomic and genotoxic response to cadmium telluride quantum dots (QDs) in human breast carcinoma cells. QD treatment induced global hypoacetylation implying a global epigenomic response. The ubiquitous responder to genotoxic stress, p53, was activated by QD challenge resulting in translocation of p53, with subsequent upregulation of downstream targets *Puma* and *Noxa*. Consequential decrease in cell viability was in part prevented by the p53 inhibitor pifithrin-α, suggesting that p53 translocation contributes to QD-induced cytotoxicity. These findings suggest three levels of nanoparticle-induced cellular changes: non-genomic, genomic and epigenetic. Epigenetic changes may have long-term effects on gene expression programming long after the initial signal has been removed, and if these changes remain undetected, it could lead to long-term untoward effects in biological systems. These studies suggest that aside from genotoxic effects, nanoparticles could cause more subtle epigenetic changes which merit thorough examination of environmental nanoparticles and novel candidate nanomaterials for medical applications.

Keywords Nanoepigenetics · Nanoparticles · p53 · Cell death · Trichostatin A · Pifithrin-α

ANGELA O. CHOI received her B.Sc. degree in Biochemistry at McGill University in Montreal, Canada. She is pursing her Ph.D. degree under the supervision of Dr. Dusica Maysinger in the Department of Pharmacology and Therapeutics at McGill University. Her research focuses on the use of nanoparticles as in vivo imaging and/or drug delivery tools in the peripheral nervous system

DR. DUSICA MAYSINGER earned her Ph.D. at the University of Southern California, Los Angeles. She did her postdoctoral studies at Max Planck Institute in Munich, Karolinska Institute in Stockholm and Oxford University, UK. Research activities focus on investigating therapeutic interventions in diabetes and neurodegenerative disorders in conjunction with nano-delivery systems. Her laboratory intensively investigates fluorescent nanoparticles (e.g., micelles and quantum dots) and their effects on signal transduction pathways in cell death and differentiation.

Electronic supplementary material The online version of this article (doi:10.1007/s00109-007-0274-2) contains supplementary material, which is available to authorized users.

Angela O. Choi and Shelley E. Brown contributed equally to the manuscript.

A. O. Choi · S. E. Brown · M. Szyf · D. Maysinger (✉)
Department of Pharmacology and Therapeutics,
McGill University,
3655 Promenade Sir William-Osler,
McIntyre Medical Sciences Building,
Montreal H3G 1Y6, Canada
e-mail: dusica.maysinger@mcgill.ca

Introduction

Nanoparticles present in our environment and used in research laboratories encompass a wide variety of self-assembly systems including micelles, nano-wires and quantum dots [1]. Quantum dots (QDs) have unique photophysical properties which can be exploited for cell tracking [2] bio- and photosensing [3] and imaging in vivo [4]. As these nanoparticles are only emerging as potential diagnostic, therapeutic, and imaging tools, limited information is available with regard to their long-term effects on different cell types in different animal and plant species [5–7].

Although the first generation of QDs seemed to be safe at doses appropriate for long-term imaging, data on their retention and/or accumulation is limited [8]. Several studies demonstrated that uncapped QDs could induce damage to mammalian cells through the generation of free radicals and DNA damage resulting in different types of cell death, including nonclassical apoptosis [9, 10]. Surface modifications with polyethylene glycol (PEG) or carboxylic acids, and encapsulation in polymeric micelles can improve the stability and biocompatibility of the QD core/shell complex [7, 11]. However, critical parameters which determine the cell's fate in the presence of QDs are not only their composite materials, but also their stability, charge, size, distribution, rates of accumulation, and elimination, as well as the status of the cellular antioxidant defense system [7, 8, 10, 12]. With this in mind, it is possible that the changes induced by QDs and other nanoparticles may not be detected through examination of overall cell morphology or through cell death analysis using standard biochemical assays. Moreover, the microenvironment in which the cells are growing is extremely important in measuring the results of QD treatment. The toxic effects of QDs are significantly minimized when cells are cultured in the presence of serum [13]; however, it is possible that the QD-induced changes under these conditions are simply not detectable, and these subtle changes may persist through cell divisions, altering the overall functions of the cell. Thus, it is necessary to examine finer cellular changes at the level of the epigenome to determine the finer effects of QDs on the cells.

Nanoparticle or metal ion-induced oxidative stress leading to cell death has been previously reported at the genomic level, but has not yet been investigated at the epigenomic level [14]. Cells undergo chromatin condensation in response to insult by cadmium and selenium, both common elements constituting QD cores [15, 16]. Induction of oxidative stress by copper or hydrogen peroxide [17] can inhibit the activity of histone acetyltransferases, thereby, leading to global hypoacetylation of histones with concurrent hyperacetylation of specific genes involved in the cell's response to oxidative stress [18]. Epigenomics, a new scientific discipline merging epigenetics and genomics, provides new insights into our understanding of genetic regulation and its role in cellular growth, differentiation, cell death, diseases, and aging [19]. Epigenetic variations operate through methylation of cytosine nucleotides in DNA and posttranslational modification of histones such as acetylation, phosphorylation, methylation, and sumoylation, all of which may be involved in modulating gene activation and expression [18]. Epigenetics can also be recognized as a mediator of the interaction between the environment and genetics [20]. QD-induced oxidative stress has been well established in different cell types [9]; however, their effects on the epigenome, including histone modifications (acetylation and methylation) and DNA methylation have not been examined.

The objective of this study was to explore QDs as gene-damaging agents and to assess if they induce epigenetic and genomic changes in human breast epithelial cancer (MCF-7) cells. Our results suggest that even small amounts of cadmium telluride (CdTe) QDs, not readily detectable inside the cells, can induce genotoxic and epigenomic changes leading to cell death. As epigenetic changes may lead to long-term reprogramming of gene expression long after the initial insult has been removed, results from "nanoepigenetic" assessments may have important implications on the future use of new nanomaterials in bioimaging and therapeutic applications.

Materials and methods

Preparation of Anionic QDs Sodium borohydride (99%; 0.8 g, 21.15 mmol) was first dissolved in water (20 ml) at 0°C. Tellurium powder (200 mesh, 99.8%; 1.28 g, 10.03 mmol) was then added portion-wise, and the mixture was stirred at 0°C under N_2 for 8 h, yielding a purple solution. The reaction mixture was kept at 4°C in the dark and used in the next step. Cadmium perchlorate hydrate (0.25 ml, 1 M aqueous solution) and 3-mercaptopropionic acid (MPA, 0.2 g, 1.884 mmol) were dissolved in 200 ml of N_2 saturated Milli-Q water. Solution pH was adjusted to 10.5 using 1 M KOH before the addition of the NaHTe solution (0.1 ml). The reaction mixture became light brown in color and was heated to reflux. Aliquots were taken as the reaction proceeded, and the fluorescence spectra were recorded to monitor the QDs growth as a function of reaction time. Photoluminescence measurements were carried out at room temperature using a Cary Eclipse Fluorescence spectrometer. The excitation wavelength was set at 400 nm. The excitation and emission slits were set at 5 nm. A green emission (λ_{em} 530 nm) was observed after 15 min. The resulting QD solution was

dialyzed against Milli-Q water for 4 h then concentrated to 15 ml using a rotary evaporator. Dialysis was performed using spectra/por molecularporous membrane tubing (Spectrum Laboratories) with a 6,000- to 8,000-Da molecular weight cutoff. QDs were precipitated using $MeOH/CHCl_3$ (1:1, *v*/*v*) then collected by centrifugation. Centrifugation was performed with Eppendorf centrifuge 5403 (10,000 rpm) and Eppendorf centrifuge 5,415 C (14,000 rpm). The QDs were washed with $MeOH/CHCl_3$ (1:1, *v*/*v*) two times then dried under vacuum. The QDs were used as solutions either in deionized water or in phosphate-buffered saline (PBS) buffer. All chemicals were purchased from Sigma-Aldrich (St. Louis, Missouri, USA).

Cell Culture Conditions Human breast adenocarcinoma cells (MCF-7) (ATCC, Rockville, MD, USA; HTB-22) were cultured in Roswell Park Memorial Institute (RPMI) 1640 media containing 10% fetal bovine serum (FBS) (Gibco, Burlington, ON, Canada). Rat pheochromocytoma cells (PC12), (ATCC, USA) were cultured in RPMI 1640 media containing 5% FBS. Cells were maintained at 37°C (5% CO_2) in a humidified atmosphere, and all media contained 1% penicillin–streptomycin and were free of phenol-red. For colorimetric assays, cells were seeded in 24-well plates (Sarstedt, Montreal, QC, Canada) at a density of 10^5cells/cm^2.

Cell Treatment Cells were washed and maintained in serum-free media (Ctrl) for 1 h before QD treatment. QDs were added to cells at a concentration of 5 μg/ml and incubated for either 4 or 24 h. In experiments involving pifithrin (PFT), pifithrin-α (2-(2-Imino-4,5,6,7-tetrahydro-benzothiazol-3-yl)-1-*p*-tolylethanone; Calbiochem, Darmstadt, Germany; 506132) was added to cells at a final concentration of 20 μM at the same time QDs (5 μg/ml) were added, and cells were incubated for 24 h. Trichostatin A (TSA; [R-(E,E)]-7-[4-(Dimethylamino_phenyl]-N-hydroxy-4,6-dimethyl-7-oxo-2,4-heptadienamide; Sigma, USA; T-8552) was added at 50 and 300 nM to the cells and incubated for 24 h.

Live Cell Imaging Images were acquired with a Zeiss LSM 510 NLO inverted microscope. Cells were grown on eight-well chambers (Lab-Tek, Nalge Nunc International, Rochester, NY, USA). QDs were added to designated wells, and the cells were incubated for 24 h. Hoechst 33342 (10 μM, 1 h, Molecular Probes H1399; λ_{ex} 350 nm, λ_{em} 461 nm) was used for nuclear staining, and this was imaged using 2-photon imaging (Ti:Sa laser set to pulse at 800 nm and BP 390–465 IR filter). Before imaging, cells were washed with PBS or with serum-free medium. No background fluorescence of cells was detected under the settings used. Images were acquired at resolutions of 512×512 and 1,024×1,024. Quadruplicate samples were analyzed in all the imaging experiments. Scan size was 146.2 μm×146.2 μm. Figures were created using Adobe Photoshop.

Electron Microscopy To assess the morphological status of mitochondria and nuclei, the cell culture media were removed by aspiration from control (untreated) and QD-exposed (24 h) cells. Media were replaced with 2.5% gluteraldehyde in 0.1 M sodium cacodylate buffer to fix the cells. The cells were kept in the fixative at 4°C for 24 h. The fixative solution was then carefully removed, and the cells were washed three times for 10 min each with 0.1 M cacodylate washing buffer. The cells were postfixed using 1% osmium tetroxide (OsO_4) in a 1.5% potassium ferrocyanide (KFeCN) solution. The cells were then kept at 4°C for 30 min to allow the cells to be immersed in the reduced OsO_4 solution. OsO_4 was then removed, and the cells were again washed with 0.1 M cacodylate washing buffer. After 10 min, the cells were dehydrated with ethanol in increments of 10% from 30% up to 90% allowing 5 min intervals in between each step. The cells were then further dehydrated twice with 100% ethanol allowing for 10 min intervals between each change. The cells were infiltrated by adding increasing amounts of epon to ethanol (in increasing increments from 1:1 to 3:1) to each of the cell wells allowing 30 min intervals between each subsequent addition. Finally, pure epon, de-aerated under vacuum (at constant pressure, not exceeding 25 psi), was added to the cell wells. The cells were allowed to sit for 1 h under vacuum to remove the ethanol residue and the air bubbles in the epon. Then, the wells were refilled with new epon and placed into an oven at 60°C for 48 h to polymerize the epon. Thin sections (0.1 μm) were prepared using an Ultracut-E ultramicrotome (Reichert-Jung, Leica Microsystems, Austria), and placed on to 200 mesh copper grids (EMS Sciences, USA). Digital images were taken with a Gatan 792 Bioscan 1k×1k Wide Angle Multiscan CCD camera (JEM-2000 FX).

Immunocytochemistry MCF-7 and PC12 cells were plated at a density of 6×10^4 on glass coverslips coated with rat tail collagen (C7661, Sigma) in a 24-well dish and treated as described above in the section on *Cell Treatment*. Cells were fixed for 30 min with 4% paraformaldehyde, blocked, and permeabilized for 1 h with 10% horse serum + 0.1% Triton-X + PBS. The cells were incubated with anti-acetylated histone 3 (Upstate) or anti-dimethyl-lysine 9 histone 3 (Upstate) polyclonal antibodies diluted 1:500 in 5% horse serum + PBS overnight at 4°C. Subsequently, the cells were washed with PBS and incubated with anti-rabbit (Alexa-568, Molecular Probes) diluted 1:400 in 5% horse serum + PBS for 1 h. Next, the cells were incubated in 2 N

HCl for 35 min at 37°C and neutralized with two washes of 0.1 M borate buffer, pH 8.5. The cells were incubated with anti-5-methyl-cytosine monoclonal antibody diluted 1:1,000 in 0.1% bovine serum albumin (BSA) + PBS overnight at 4°C. Finally, the cells were incubated with anti-mouse (Alexa-633, Molecular Probes) diluted 1:400 in 5% horse serum + PBS for 1 h. Cells treated with pifithrin were first incubated with anti-p53 (1:500, sc-6243, Santa Cruz Biotechnology, CA, USA) polyclonal antibody, and then incubated with anti-mouse FITC-conjugated IgG secondary antibody (3846SA, Gibco, MD, USA). Visualization was performed using a Zeiss Axioplan 2 Imaging fluorescence microscope, equipped with a high-resolution color digital camera and connected to a computer with the Zeiss Axiovision 4.1 Software (Zeiss Canada).

Histone Extraction Total histones were extracted from cells by resuspending the cells in 4 ml NP-40 lysis buffer (10 mM Tris, pH 7.4, 10 mM NaCl, 3 mM $MgCl_2$, 0.5% NP-40), followed by a 5-min incubation at 4°C, and spun down at 1,000 rpm for 5 min, 4°C. The supernatant was discarded, and the pellet was again resuspended in 4 ml NP-40 lysis buffer, and spun for 5 min at 1,000 rpm, 4°C. After removing the supernatant, the pellet was resuspended in 20 μl histone extraction buffer [10 mM Tris, pH 7.4, 10 mM Na-Butyrate, 4 mM $MgCl_2$, 0.1 mM phenylmethylsulphonyl fluoride (PMSF)] and 20 μl 0.8 N HCl, and incubated overnight at 4°C. The samples were spun for 10 min at 12,000 rpm at 4°C, and the supernatant containing the histones was transferred to a new tube. Protein concentration was determined using a standard Bradford assay (BioShop). Western blots were performed as described below.

Reverse Transcription and PCR Amplification Total RNA was extracted from cells using a standard guanidinium procedure. cDNA was synthesized in a 20-μl reaction volume containing 2 μg of total RNA, 40 U of Moloney murine leukemia virus reverse transcriptase (MBI), 5 μM random primer (Roche Applied Science), 1 mM of each of the deoxynucleotide triphosphates, and 40 U of RNase inhibitor (Roche Applied Science). mRNA was denatured for 5 min at 70°C, the random primers were annealed for 10 min at 25°C, and the mRNA was reverse-transcribed for 1 h at 37°C. The reverse transcriptase was heat-inactivated for 10 min at 70°C, and the products were stored at −20°C until use. Polymerase chain reaction (PCR) amplification was performed in a 25-μl reaction mixture containing 1.0 μl of synthesized cDNA product, 2.5 μl of 10× PCR buffer, 1.5 mM $MgCl_2$, 0.2 mM deoxyribonucleotide triphosphate (dNTP), 1 U of *Taq* polymerase (all from Fermentas) and 0.5 μM of each primer. Samples were taken every 2 cycles from 16 to 28 cycles to ensure the amplification was in the linear range. The primer sequences used are listed in a Table 1 of the Supplementary Material.

Subcellular Fractionation Subcellular fractionation was performed by using the ApoAlert cell fractionation kit (BD Biosciences, Mississauga, ON, Canada) according to the manufacturer's instructions.

Western Blotting Of the subcellular fractionation extracts, 25 μg, or 5 μg of histone extracts were loaded onto a gradient sodium dodecyl sulfate-polyacrylamide gel electrophoresis (SDS-PAGE) gel and transferred to a nitrocellulose membrane. Membranes were blocked with 5% milk or 5% BSA + 0.5% Tween-20 + TBS for 1 h and incubated with the primary antibody in blocking solution for 1 h. After two washes with 0.1% Tween-20 + TBS, the membranes were incubated with the secondary anti-rabbit diluted 1:4,000 in 5% milk + 0.5% Tween-20 + TBS for 1 h. After three washes with 0.1% Tween-20 + TBS, the membranes were exposed to film, and a single band was observed. The primary antibodies used were anti-p53 (sc-6243, 1:500), anti-Bax (sc-493, 1:500), anti-PCNA (sc-56, 1:500) from Santa Cruz Biotechnology, anti-phospho-p53 (Ser15–9284, 1:1000) from Cell Signaling Technology, anti-actin (MAB1501R, 1:1000) from Chemicon, anti-cox IV (1:500) from ApoAlert kit (BD Biosciences, Canada), anti-acetylated histone 3 (1:2500) and anti-histone 3 (1:10,000) from Upstate.

Cell Viability as determined by MTT Assay and Cell Counting Colorimetric 3-(4,5-dimethylthiazol-2-yl)-2,5-diphenyl tetrazolium bromide (MTT) (Sigma), assays were performed to assess the mitochondrial activity of cells treated as described above. After 24 h treatment, media was removed and replaced with drug-free, serum-free media. MTT (final concentration of 455 μg/ml; 50 μl of 5 mg/ml stock solution) was added to each well (final volume 550 μl), and cells were then incubated for 1 h at 37°C, after which, cell media was removed, and cells were lysed with the addition of dimethyl sulfoxide (DMSO). Formazan is thus dissolved, and absorbance was measured at 595 nm using a Benchmark microplate reader (Bio-Rad, Mississauga, ON, Canada). Cell viability was determined as the number of viable cells according to standard cell counting protocol using the Trypan blue dye. Cells were treated with drugs and QD as indicated in individual figure legends. Cells were detached using trypsin/EDTA (Gibco, Montreal, Canada). Staining with trypan blue dye (Gibco) indicates whether cells were dead (blue) or viable (clear). All measurements were taken in triplicate from three or more independent experiments.

Statistical Analysis Data were analyzed using SYSTAT 10 (SPSS, Chicago, IL, USA). Statistical significance was determined by Student's *t* tests with Bonferroni correction. Differences were considered significant where $*p<0.05$, $**p<0.01$, $***p<0.001$.

Results

Cell exposure to quantum dots induces changes at the nuclear and mitochondrial levels

Nanoparticles, such as certain quantum dots (QDs), cause cell damage and death [6, 9, 10]. Depending on the cell type, intensity, and duration of QD-insult, different components of cell death mechanisms are activated by the formation of reactive oxygen species (ROS), induction of lipid peroxidation, and intracellular organelle or DNA damage [9, 10]. Confocal micrographs in this study show cadmium telluride (CdTe) QD interference with nuclear morphology (Fig. 1). Live cell imaging with a fluorescent dye, Hoechst 33342, clearly showed reorganized nuclear DNA in cells treated with QDs for 24 h (Fig. 1b), and electron micrographs confirmed this reorganization of nuclear content (Fig. 1d). Nuclear shrinkage, chromatin condensation and reorganization, and mitochondrial functional impairments (Fig. 1; Supplementary Material, SFig. 1 and SFig. 2) are associated with multiple pathways leading to cell death of different types [9, 21]. Damage to the mitochondrial membranes and partial elimination of mitochondrial cristae were also observed in electron micrographs (Fig. 1f). In some instances, hypertrophic mitochondria were visible, and disorganized cristae were also observed. These disruptions of mitochondrial integrity may explain enhanced membrane permeabilization and QD-induced impaired mitochondrial functions as previously reported by our group [10]. However, cell exposures to low concentrations of CdTe QDs and in the presence of serum lead to minor chromatin reorganization without consequent cell death.

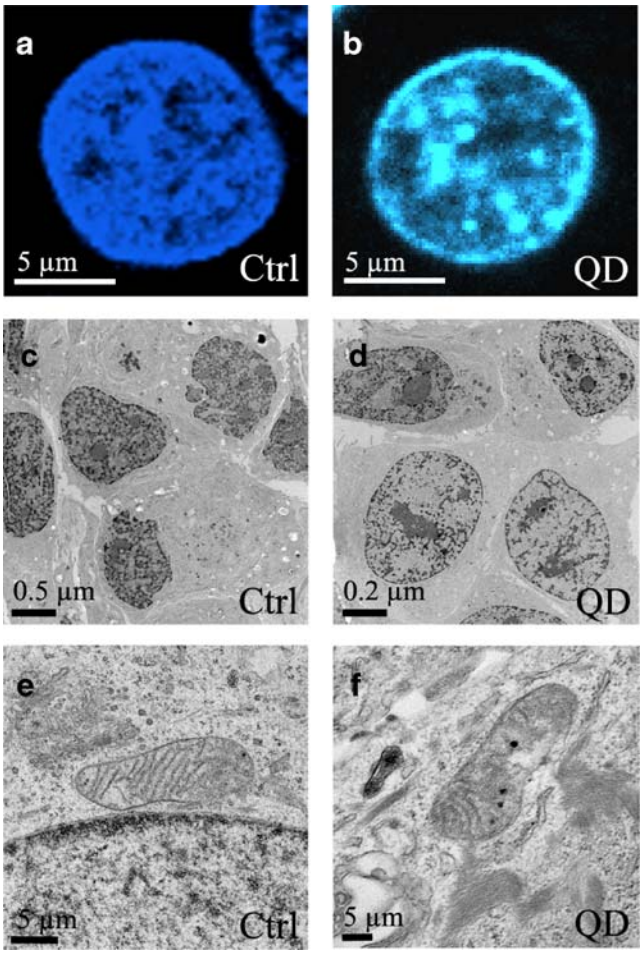

Fig. 1 Nuclear and mitochondrial changes induced by QD treatment detected by confocal and electron microscopy. Confocal micrographs of MCF-7 cells untreated (Ctrl) or treated with CdTe QDs for 24 h (QD). Nuclei were stained with Hoechst 33342 (*blue*) and show chromatin condensation in QD-treated cells (**b**) compared to untreated cells (**a**). *Scale bars* represent 5 µm. Electron micrographs of MCF-7 cells treated with QDs for 24 h (QD) show reorganization of nuclear content (**d**) and loss of mitochondrial cristae (**f**) compared to untreated cells (**c**, **e**). *Scale bars* represent 5 µm (**e**, **f**) 0.5 µm (**c**), 0.2 µm (**d**)

The nucleus undergoes chromatin condensation and global hypoacetylation of histone 3 after quantum dot treatments in MCF-7 cells

Live cell imaging of nuclei, electron micrographs, and three-dimensional nuclei reconstruction, [22] all indicated nuclear rearrangements induced by QDs (Fig. 1), but could not explain the cause or extent of these nuclear changes. DNA fragmentation and nicking due to QD-insult have been previously reported by others [23], but we now show that QDs can also induce changes at the epigenetic level. We assessed two histone modifications, specifically acetylated histone 3 and di-methylated lysine 9 on histone 3, as well as methylated DNA. Untreated MCF-7 cells (Ctrl) display typical organization of 5-methyl-cytosine (5-mC) localized on the periphery of the nucleus, colocalizing with the repressive dimethyl-lysine 9 mark on histone 3 (diMeK9-H3; Fig. 2a), and also showing colocalization with the acetylated histone 3 (Ac-H3), which marks active euchromatin (Fig. 2b). Upon treatment with QDs for 24 h, we see a distinctive change in the structure of the DNA typical of chromatin condensation (Fig. 2a and b). As expected, the dimethyl-lysine 9 of histone 3 remained colocalized with 5-mC (Fig. 2a). Surprisingly, the signal for acetylated histone 3 was significantly decreased within the cells treated with QDs, although the immunoreactivity was successful, as indicated by the cell in the bottom left corner which was unaffected by the QDs (Fig. 2b). The global

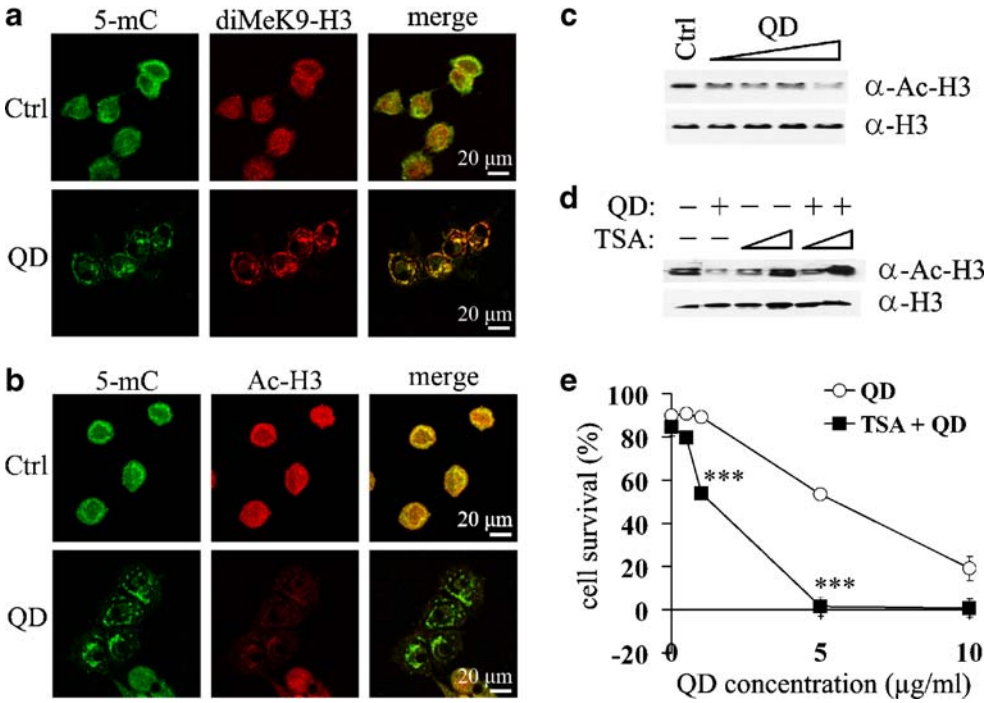

Fig. 2 The nucleus undergoes chromatin condensation and hypoacetylation of histone 3 after QD treatment in MCF-7 cells. MCF-7 cells were grown on rat tail collagen coated-glass coverslips, untreated (Ctrl) or treated for 24 h with 5 μg/ml of CdTe QDs (QD) and stained with anti-5-methylcytosine (5-mC) antibody, followed by Alexa-568-conjuated anti-mouse secondary antibody (*green*). The same cells were also stained with anti-dimethyl-lysine 9, histone 3 (diMeK9-H3) anti-body (**a**) or anti-acetylated histone 3 (Ac-H3) antibody (**b**), followed by Alexa-633 antibody (*red*). Merged confocal micrographs of 5-mC and diMeK9-H3 or acetylated histone 3 are shown, respectively. *Scale bars* represent 20 μm. **c** MCF-7 cells were untreated (Ctrl) or treated with 0.5, 1.0, 5.0, or 10.0 μg/ml of QDs for 24 h. Histones were extracted and assayed by Western blot with an antibody directed against acetylated histone 3 (α-Ac-H3; top panel). The membrane was stripped and re-probed with an antibody directed against histone 3 as a loading control (α-H3; *bottom panel*). **d** MCF-7 cells were untreated (Ctrl) or treated with 10.0 μg/ml of QDs, with or without 50 or 300 nM TSA, for 24 h. Histones were extracted and assayed by Western blot with the same antibodies as in (**c**). Cell survival was assessed using cell counting (**e**) after cell treatment with increasing concentrations of QDs (0.5–10.0 μg/ml) with (*solid squares*) or without (*open circles*) 50 nM of TSA. Values represent means ± SEM from triplicate measurements obtained from three independent experiments. ***$p<0.001$ where significance was found between the QD and the TSA+QD groups

hypoacetylation was also detected using Western blots with an antibody directed against acetylated histone 3 (Fig. 2c). Western blot analyses of QD concentration-dependent hypoacetylation revealed detectable hypoacetylation at very low concentrations of QDs (<5 μg/ml), despite the absence of cell death-associated morphological changes at these low doses. The decrease in hypoacetylation, however, was most evident in cells treated with a high dose of QDs (10 μg/ml; Fig. 2c, lane 5). It is likely that not all cells are equally affected by low QD concentrations (<5 μg/ml), resulting in a masking of the effects when an entire cell population is analyzed.

We next assessed whether this QD-induced hypoacetylation can be reversed using a pharmacological agent, trichostatin A (TSA), which increases the global levels of acetylated histones by inhibiting histone deacetylases (HDACs). Low (50 nM) and high (300 nM) dose TSA was added to MCF-7 cells with or without QDs (10 μg/ml) for a period of 24 h, and the effects on global histone acetylation was assessed using Western blots. Cells treated with a low dose of TSA (50 nM) and QDs show a clear increase in the levels of histone acetylation compared to cells treated with QDs alone (Fig. 2d, lanes 2 and 5). This hyperacetylation was even more apparent at a higher concentration of TSA (300 nM) in the presence of QDs (Fig. 2d, lane 6). However, despite altering the histone acetylation status using TSA, cells were not protected from QD-induced cytotoxicity as assessed by cell counting (Fig. 2e). Previous studies have shown that TSA can reduce cancer cell viability [24]; nevertheless, at low concentrations (≤50 nM), no significant cell death was observed in MCF-7 cells. Interestingly, concomitant cell treatment with low dose TSA (50 nM) and QDs (0.5, 1, 5, and 10 μg/ml) induced significantly more cytotoxicity than treatment with QDs alone (Fig. 2e; $p<0.001$). Taken together, these findings suggest that the balance of histone acetylation is critical in maintaining cell viability and that both hyper- and hypoacetylation can lead to cell death.

Quantum dots induce an increase in the mRNA levels of p53-target genes Bax, Puma, and Noxa

Global hypoacetylation in QD-treated cells suggests reduced gene transcription, so we selected several genes involved in scavenging ROS, and triggering or preventing apoptosis, and examined their mRNA levels through reverse transcriptase polymerase chain reaction (RT-PCR). For all genes examined through RT-PCR, samples were taken at three different cycle numbers to demonstrate the samples are within the linear range of amplification (Fig. 3, ethidium bromide gels). The middle samples were used for quantification. Fumarase and superoxide dismutase 1 (SOD-1) are endogenous enzymes involved in reducing intracellular ROS [25, 26]. The *fumarase* mRNA levels did not significantly increase after QD treatment (Fig. 3a). The addition of the HDAC inhibitor TSA alone did not change the levels of *fumarase*; however, in combination with QDs, there was a large increase in the mRNA levels, indicating there may be a synergistic effect of these two treatments, despite the opposing effects on the histone acetylation levels (Fig. 2). There was a significant increase in SOD-1 levels after QD treatment (Fig. 3a; $p<0.01$ compared to Ctrl), indicating an early SOD-1 response to QD treatment. On the other hand, TSA alone resulted in a significant decrease in SOD-1 levels ($p<0.01$), indicating that TSA-induced cellular stress does not affect the same cell-protecting antioxidant pathway. QD treatment in combination with TSA restored the levels of SOD-1 to that of QD treatment alone (Fig. 3a).

In addition, we examined the mRNA levels of some anti-apoptotic genes to determine whether there was a reduction after QD treatment, thereby, promoting cell death. The mRNA levels of two genes involved in preventing cell death, *cIAP-1* (Inhibitor of apoptosis) and *Hsp70* (Heat shock protein 70), were significantly reduced in QD-treated cells (Fig. 3b). Moreover, *GPx* (glutathione peroxidase) mRNA expression was completely suppressed after QD treatment ($p<0.05$). The downregulation of these three genes was also observed after TSA treatment alone, and when cells were treated with a combination of TSA and QDs, the mRNA levels of *GPx* and *Hsp70* remained low. Interestingly, the mRNA levels of *cIAP-1* were significantly induced by combined treatment with QDs and TSA ($p<0.001$), whereas TSA itself downregulated *cIAP-1* mRNA levels suggesting an opposing effect of QDs and TSA.

Intracellular ROS produced by QDs can trigger the accumulation of Bax (Bcl-2 associated X) proteins to the

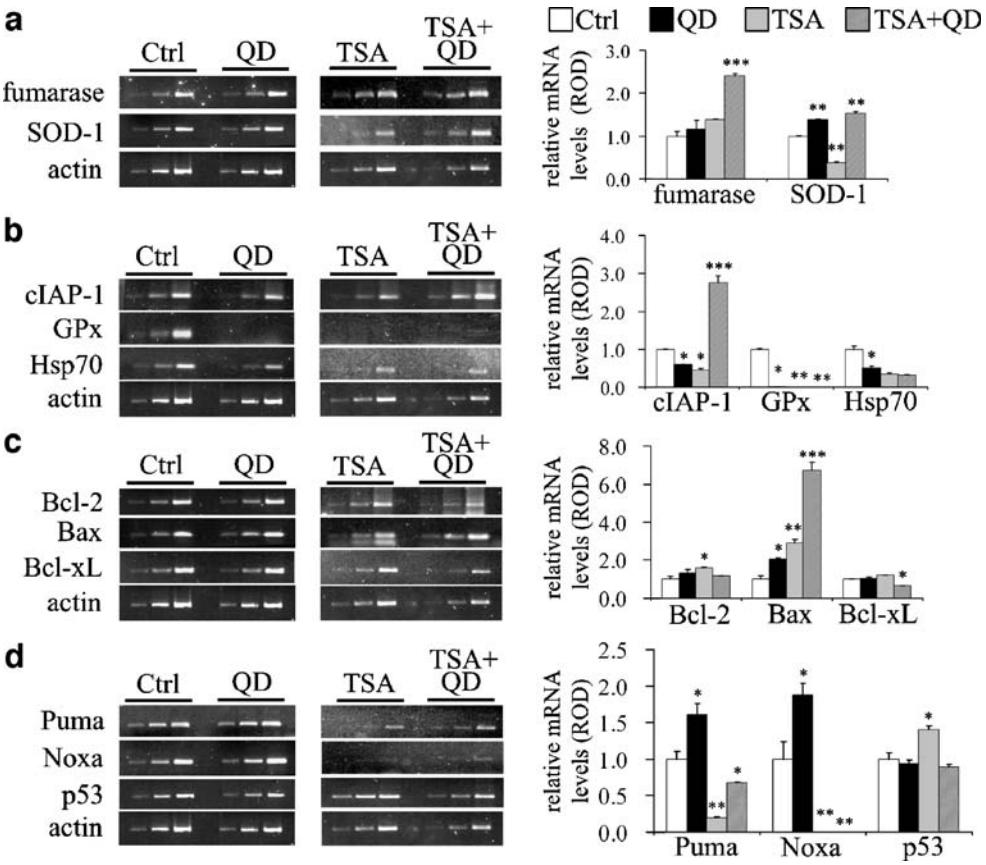

Fig. 3 QD treatment induces increased mRNA levels of the genes *Puma*, *Noxa*, *and Bax*. Total RNA was extracted and cDNA synthesized from MCF-7 cells untreated (Ctrl), treated with CdTe QDs (QD), treated with TSA (TSA), or treated with CdTe QDs and TSA (TSA+QD) for 24 h. RT-PCR amplification of the cDNA of *fumarase* and *SOD-1* (**a**), *cIAP-1*, *GPx* and *Hsp70* (**b**), *Bcl-2*, *Bax*, and *Bcl-xL* (**c**) and *Puma*, *Noxa*, and *p53* (**d**). *Actin* was used as a control to demonstrate equal loading. The amplification of the PCR products was determined to be in the linear range by taking three samples every two cycles. The middle samples were quantified and normalized to actin, shown as relative mRNA levels by measuring relative optical density (ROD). Values represent means ± SEM from triplicate measurements obtained from two to three independent experiments (*$p<0.05$, **$p<0.01$, ***$p<0.001$ compared to Ctrl)

mitochondria and induce the release of various factors leading ultimately to apoptosis. Contrary to Bax, Bcl-2, and Bcl-xL are anti-apoptotic factors involved in preventing cell death [27]. Interestingly, *Bcl-2* and *Bcl-xL* mRNA levels were unaffected, whereas the levels of *Bax* mRNA were significantly increased in QD-treated cells (Fig. 3c; $p<0.05$), indicating that Bax may be involved in inducing apoptosis through increasing the overall levels within the cell, promoting a pro-apoptotic state. The fact that selective transcripts were induced suggests that the response to QDs may be gene-selective for pro-apoptotic genes. The mRNA levels of *Bcl-2* and *Bcl-xL* after TSA treatment was similar to that of the QD treatment alone. *Bax* mRNA levels, on the other hand, were increased to a higher level than QD treatment alone, and concomitant treatment shows an additive increase of *Bax*. Therefore, it appears that Bax is involved in both QD- and TSA-induced cell deaths.

As Bax has been previously shown to be activated through p53 [28], we examined whether the levels of *p53* mRNA are also increased in QD-treated cells and inducing a p53-dependent cell death. While we did not observe any change in the mRNA levels of *p53* (Fig. 3d) after QD treatment alone, there was an increase in *p53* mRNA levels after TSA treatment ($p<0.01$). This effect was suppressed when cells were treated with both TSA and QDs. On the other hand, cells treated with QDs showed a significantly increased transcription of *Puma* (p53-upregulated modifier of apoptosis) and *Noxa* (NADPH oxidase activator 1) (Fig. 3d; $p<0.05$), two genes that are involved in apoptosis induction and are regulated by the activity of p53 [29]. TSA treatment completely suppressed the expression of these genes, and the combination of QDs plus TSA resulted in a reactivation of *Puma*, but not *Noxa* mRNA expression. This finding indicates that p53-regulated genes, such as *Bax*, *Puma*, and *Noxa*, may play important roles in the induction of cell death by QDs in MCF-7 cells.

Quantum dot treatment induces an increase in overall p53 protein levels, its posttranslational modification by phosphorylation, and its inter-organelle translocation in MCF-7 cells

Puma, *Noxa*, *Bax,* and other pro-apoptotic genes are regulated at the transcriptional level by activated (via phosphorylation of) p53 [29]. As we saw no change in the mRNA levels of *p53* upon QD treatment, we asked whether there is more phosphorylated p53 protein in QD-treated vs untreated cells. Interestingly, QDs induced a dramatic increase in phosphorylated p53 protein (P-p53) detectable in the nucleus, cytosol, and mitochondria as assessed with Western blots using an antibody specific for phosphorylated p53 (Fig. 4a and b). It is thus conceivable that the induction of *Puma*, *Noxa*, and *Bax* was due to the activation of p53 and increased binding of the P-p53 to the promoters of these genes. Further to changes at the mRNA level for *Bax*, we were interested in determining whether

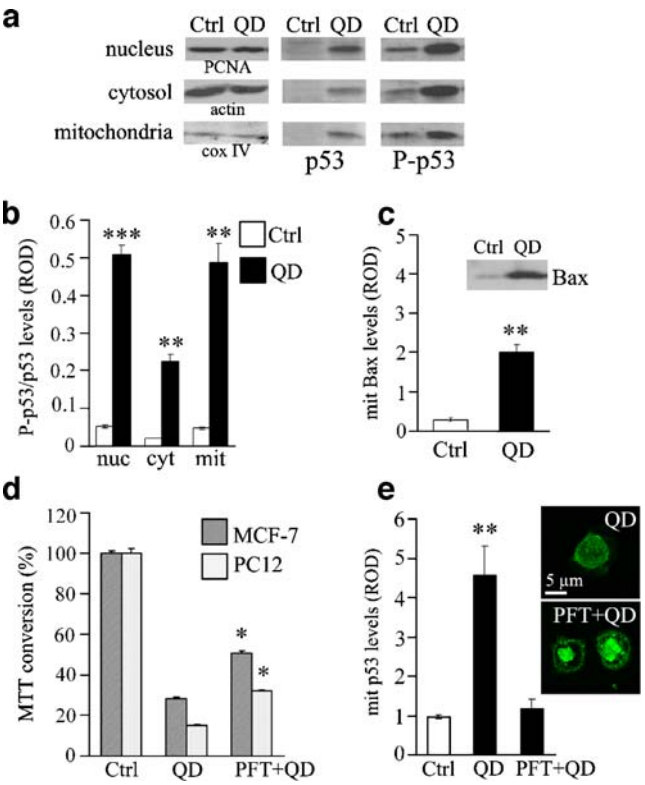

Fig. 4 QD treatment induces increased protein levels of p53, phosphorylated-p53, and Bax. Pifithrin protects cells from QD-induced cell death through inhibition of p53 translocation to the mitochondria. **a** MCF-7 cells, untreated (Ctrl) or treated with 5 µg/ml CdTe QDs for 3 h (QD) were lysed and isolated into nuclear, cytosolic, and mitochondrial fractions. Western blot analysis of phosphorylated-p53 (P-p53) and p53 proteins in each subcellular fraction are shown. PCNA (nucleus), actin (cytosol), and cox IV (mitochondria) were used to demonstrate equal loading. **b** Quantification of the protein signals shown as the ratio of P-p53 to p53 levels, corrected with the respective subcellular loading controls (*ROD* Relative optical density). *nuc* Nuclear fraction, *cyt* cytosolic fraction, *mit* mitochondrial fraction. **c** Western blot analysis of Bax protein from the mitochondrial fraction of MCF-7 cells treated with QDs for 24 h (QD). Protein quantification of Bax is shown in relative optical density corrected with cox IV as the loading control. **d** Cell viability of MCF-7 and PC12 cells treated for 24 h with QDs alone (QD) or concomitantly with pifithrin (PFT+QD) was assessed with the MTT assay. **e** Quantification of p53 protein levels based on Western blot analysis of the isolated mitochondrial fraction of PC12 cells treated with QDs alone (QD) or concomitantly with pifithrin (PFT+QD). Values are corrected with cox IV loading control. Immunocytochemistry of PC12 cells treated with QDs alone (QD) or concomitantly with pifithrin (PFT+QD) and stained with anti-p53 antibody, followed by FITC antibody (*green*). Scale bar represents 5 µm. Values represent means ± SEM from triplicate measurements obtained from two to three independent experiments. *$p<0.05$, **$p<0.01$, ***$p<0.001$ where significance was found compared to Ctrl

these changes were accompanied with an increase at the protein level. Western blot analysis of the isolated mitochondrial fraction and using an antibody specific against Bax revealed that there was no significant change in the protein levels of Bax after 3 h of QD treatment (data not shown), but there was a markedly enhanced intensity of the immunoreactive band in the mitochondria after QD treatment for 24 h (Fig. 4c).

Translocations of the pro-apoptotic proteins to mitochondria, such as p53 and Bax have been shown to lead to cell death [30]. To study whether this translocation occurs upon QD treatment, we employed two pharmacological agents which are known to alter translocation of these proteins, namely, pifithrin-α (p53 inhibitor; PFT) and pentapeptide V5 (Bax-inhibiting peptide, VPMLK) [31, 32]. MCF-7 and PC12 cells treated concomitantly with QDs and PFT resulted with significantly increased cell survival, by 22.4±1.3% ($p<0.05$) and 16.8±0.4% ($p<0.05$), respectively, compared to cells treated only with QDs (Fig. 4d). Western blot analysis of the mitochondrial fraction of PC12 cells treated with QDs alone or concomitantly with PFT, and using an antibody against p53, showed that in the presence of PFT, p53 protein levels are decreased (Fig. 4e). Immunocytochemistry analysis of cells with the same treatments confirms that p53 inter-organelle (or intracellular) movement is limited in the presence of its inhibitor (PFT). These findings suggest that QD-induced cell death involves at least in part p53 translocation to the mitochondria. In contrast, treatment of cells with the pentapeptide V5 which inhibits Bax translocation did not prevent or rescue the cells from QD-induced cytotoxicity (unpublished observation), indicating that Bax translocation does not significantly contribute to the QD-induced cell death in MCF-7 cells.

Discussion

Many nanoparticles may seem innocuous, but their sequestration in tissues and long-term exposure to the (bio) environment can destabilize them. Cell exposure to unstable, poorly capped or coated nanoparticles can impair cell functions [6, 9, 10]. This study shows an example of nanoparticle-induced cellular changes, and the interlinking mechanisms underlying these changes at the genomic, non-genomic, and epigenetic levels. We provide evidence for p53 involvement at these three levels in cadmium telluride QD-induced MCF-7 cell damage. This study is only an initial step in the unexplored field of epigenetic changes by nanoparticles, which goes far beyond the assays employed here.

The nucleus acts as a hub to most cellular signaling pathways, including both survival and death signals, as its regulation of gene transcription is, in turn, regulated by activators and inhibitors of these same pathways. In light of the fact that chromatin reorganization was observed in QD-treated cells (Fig. 1), we report that this chromatin condensation is associated with changes in the epigenome after QD insult. Global hypoacetylation of histones observed in cells treated for 24 h with QDs (Fig. 2) is linked with decreased gene transcription, and suggests a global decrease in transcription which could include anti-apoptotic genes. RT-PCR evaluation of the transcription of anti-apoptotic genes, such as *cIAP-1*, *GPx*, and *Hsp70*, were indeed decreased after QD treatment. The most marked reduction of mRNA was found for *GPx* (glutathione peroxidase), suggesting that it plays a critical role in cell protection from QD-induced oxidative stress. Indeed, several studies, including a recent one by Robertson's group, showed that GPx exerts cytoprotective effects in pancreatic islet beta cells against hyperglycemia and ROS by catabolizing excess H_2O_2 and intracellular lipid peroxides [33]. On the other hand, the mRNA levels of other anti-apoptotic genes *fumarase* and *SOD-1* were actually upregulated in the presence of QDs in contrast to the global change in acetylation. Pro-apoptotic genes including *Bax*, *Puma*, and *Noxa*, were also upregulated in the presence of QDs. The fact that several mRNA induced by genotoxic stress are also induced by QDs in spite of the global hypoacetylation, suggests that in parallel to global chromatin reconfiguration characteristic of repressed transcriptional activity, distinct cytoprotective pathways are also activated in response to the genotoxic challenge of QDs. It is still unknown, however, whether the global hypoacetylation and the specific activation of certain pathways are a coordinated response to the QD challenge, or whether QD-induced histone hypoacetylation is causative of the cell death, nor is it known what mechanism is driving this bimodal response to QD challenge. Future studies should determine the long-term consequences of the global reconfiguration of chromatin to long-term epigenetic programming of specific genes.

Typically, condensed chromatin is associated with hypoacetylated histones, and numerous reports have demonstrated that cells undergoing apoptosis have hypoacetylated histones [34]. Therefore, the hypoacetylation observed upon QD treatment is typical of the induction of an apoptotic response (Fig. 2a). Paradoxically, histone deacetylase (HDAC) inhibitors are currently being used as anticancer therapy, and trichostatin A (TSA), a potent HDAC inhibitor, has been shown to induce cell death [24]. However, it has been suggested that the induced cell death is not due to the effects on global histone acetylation levels but rather due to the activation of several pro-apoptotic genes. Indeed, we observed an increase in the mRNA levels of the pro-apoptotic *Bax* gene after TSA treatment. Other

pro-apoptotic genes which are induced by QDs were actually repressed by TSA treatment, thus, indicating that QD-induced cell death and TSA-induced cell death most likely proceed via different pathways.

The induction of global hypoacetylation during apoptosis would indicate an overall decrease in gene expression as the genome is less accessible to transcription factors. Therefore, this brings about the question of how individual genes may be upregulated during apoptosis, as we have seen that the increased mRNA levels of *Bax*, *Puma*, and *Noxa* (Fig. 3) may co-exist with the global hypoacetylation of histones and chromatin condensation. p53 is able to recruit histone acetyltransferases (HATs) such as p300, and together, they act to induce gene expression of p53-dependent genes [35]. Therefore, it is possible that despite the global hypoacetylation observed after QD treatment, local p53 recruitment may bring about local hyperacetylation to allow for increased mRNA production.

As the transcription of the genes examined here is regulated by p53 which is a nodal coordinator of the apoptotic response to genotoxic stress [36], we studied the response of p53 to the QD challenge. *p53* mRNA was not upregulated in response to QD treatment (Fig. 3d). We therefore determined whether QD treatment resulted in activation of p53 by posttranslational mechanisms. It is well established that upon cellular stress and DNA damage, p53 is phosphorylated at the serine residues in the N-terminal and acetylated at the lysines in the C-terminal [28]. This activated form of p53 is then freed from its nuclear binding complex, HDM2/MDM2 (human/murine double minute 2), and binds

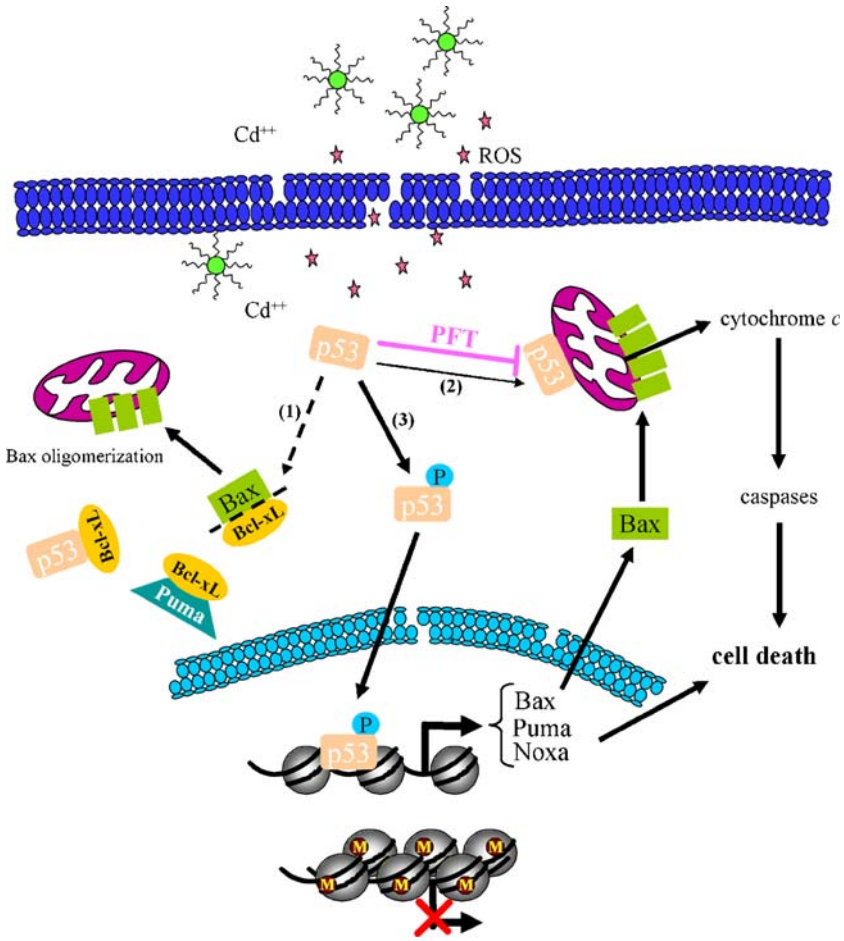

Fig. 5 Scheme showing changes at the cellular epigenetic and genomic levels induced by QDs. QDs release reactive oxygen species (ROS) and free cadmium ions extra- and intracellularly, triggering changes in the epigenome through chromatin condensation and histone hypoacetylation. QDs induce increased protein levels and activation of the transcription factor p53 resulting in: *1* cytosolic p53 directly activating Bax by freeing it from its binding proteins and facilitating the mitochondrial accumulation of Bax; *2* p53 proteins can mis-translocate to the mitochondria, leading to membrane permeabilization and consequential cell death. Pifithrin-α (PFT), a specific inhibitor of p53, can prevent this mis-translocation, and thereby, can partially prevent QD-induced cell death; *3* activated (phosphorylated) p53 induces the transcription of pro-apoptotic genes, including *Bax*, *Puma*, and Noxa. Bax proteins accumulate and oligomerize at the mitochondrial membrane, forming pores and releasing cytochrome *c*, leading to cell death. Puma facilitates Bax mitochondrial accumulation by occupying Bax-binding proteins (i.e., Bcl-xL), freeing cytosolic Bax

DNA with higher affinity, thereby improving its efficiency as a transcription factor [35]. Among the genes upregulated by p53 are *Bax*, *Puma*, and *Noxa*, which are well established and essential inducers of p53-dependent apoptosis [29]. We show here that there is an increase in activated p53 (P-p53) upon 3 h of QD treatment, and this activated p53 is particularly abundant in both the nuclear and mitochondrial fractions (Fig. 4a and b). Our findings also showed that there is an upregulation of Bax proteins after the increase of activated p53 in QD-treated cells, which is consistent with the known downstream effects of p53 activation.

Apart from its role as a transcription promoter, cytoplasmic p53 also directly activates Bax, a member of the pro-apoptotic Bcl-2 family, by displacing Bax from its binding protein Bcl-xL [28], therefore, freeing Bax in the cytoplasm. Free Bax translocates and accumulates at the mitochondria, disrupts the mitochondrial membrane potential, releases cytochrome *c* leading to caspases activation, and ultimately cell death [28]. Other activators of Bax include the p53-dependent Puma and Noxa, both BH3-only family members, which also bind Bcl-xL in the cytoplasm. After induction, Puma and Noxa associate with various other pro-apoptotic factors, including BH3 domain proteins [29], indicating that these factors play an important role in the apoptotic pathway.

p53-mediated cell death is not necessarily dependent on new protein synthesis [28] as recent studies demonstrate that transcriptional and cytoplasmic functions of p53 are interlinked. Translocation of cytoplasmic p53 to the mitochondria can lead to permeabilization of mitochondrial membranes, leading to the release of cytochrome *c*, and ultimately cell death [30]. Our studies with a pharmacologic agent, pifithrin-α, corroborate the cytoplasmic role of p53. Pifithrin (PFT) acts as a specific inhibitor of p53 transcriptional activity, and inhibits the translocation of cytoplasmic p53 to the mitochondria and the nucleus, thereby protecting cells from different insult stimuli, including ischemia and oxidative stress [31]. Our results indicate that PFT abolished the presence of p53 at the mitochondria, and retained inactive p53 at the nucleus, but it did not completely prevent QD-induced cell death (Fig. 4d and e). These findings suggest that QD-induced cytotoxicity involves, at least in part, p53 subcellular translocation and consequent transcriptional action and/or mitochondrial membrane permeabilization, which could contribute to the morphological changes observed in electron micrographs (Fig. 1f).

This study shows that exposure of MCF-7 cells to hardly detectable intracellular QDs can cause epigenetic changes and trigger p53 posttranslational modifications and its translocation to mitochondria (Fig. 5). The activation of p53 results in upregulation of several p53-regulated pro-apoptotic genes: *Puma*, *Noxa*, and *Bax*. These data pose the question of what might be the consequences to normal tissues of long-term, subthreshold exposures to QDs. Interestingly, in addition to the p53 pathway response to the QD challenge, we observed a global epigenomic response of loss of H3-acetylation. This histone hypoacetylation is likely associated with the decreased transcription of cytoprotective genes (i.e., *cIAP-1*, *GPx*, and *Hsp70*), as observed in QD-treated cells. Altogether, QD treatment triggered pro-apoptotic pathways, and at the same time, downregulated anti-apoptotic genes, thereby promoting cell death. Whether the histone hypoacetylation is the cause of QD-induced cell death or whether this occurs in concert with other histone changes, it remains that QD treatment causes an overall chromatin restructuring, associated with severe impairment of cell functions. The restructuring of chromatin is known to be associated with programming of gene expression, and our data suggest that epigenetic modifications of targeted regulatory sequences, in response to subtle but continuous nanoparticle-associated environmental insults, might serve as a source of epigenetic variations in gene expression and cell functions.

The effects of nanoparticles on chromatin structure described here point towards possible intermediate processes that dynamic environmental conditions such as nanoparticles exposure may imprint on the gene expression patterns with long-term consequences. Epigenetic changes induced by nanoparticles similar to those described in the present studies merit further investigations addressing the question of how nanoparticles impact on the epigenome in many other cells in vitro, and more importantly, in vivo. Future experiments will determine whether the global hypoacetylation response is triggered by the same mechanisms which target the p53 damage-sensing pathway or whether other mechanisms are involved and if the changes observed here persist long after the QD insult is removed. This could have long-term effects on health, which may not be detected by acute toxicity screens. With the growing array of nanotechnological products and wealth of current nano-structures, such as nanotubes, nano-wires, and other different self-assembly entities, it is important to identify key factors and establish reliable tests, including epigenetic screening (“nanoepigenetics”) to predict toxicity and provide guidance for creating safe nanomaterials.

Acknowledgements The authors would like to thank Jacynthe Laliberté for her help with the confocal microscopy and Jeannie Mui for her help with the electron microscopy. Also, the authors would like to thank Dr. Alain Niveleau for providing the anti-5-methyl-cytosine antibody and Dr. Jasmina Lovriç for scientific discussions. SEB is supported by a Doctoral Research Award from CIHR. These studies were supported by grants from the NCIC awarded to MS and grants from CIHR and JDRF awarded to DM.

References

1. Pinaud F, Michalet X, Bentolila LA et al (2006) Advances in fluorescence imaging with quantum dot bio-probes. Biomaterials 27:1679–1687
2. Courty S, Luccardini C, Bellaiche Y, Cappello G, Dahan M (2006) Tracking individual kinesin motors in living cells using single quantum-dot imaging. Nano Lett 6:1491–1495
3. Bakalova R, Ohba H, Zhelev Z, Ishikawa M, Baba Y (2004) Quantum dots as photosensitizers? Nat Biotechnol 22:1360–1361
4. Du W, Wang Y, Luo Q, Liu BF (2006) Optical molecular imaging for systems biology: from molecule to organism. Anal Bioanal Chem 386:444–457
5. Maysinger D, Lovric J, Eisenberg A, Savic R (2007) Fate of micelles and quantum dots in cells. Eur J Pharm Biopharm 65: 270–281
6. Hardman R (2006) A toxicologic review of quantum dots: toxicity depends on physicochemical and environmental factors. Environ Health Perspect 114:165–172
7. Nel A, Xia T, Madler L, Li N (2006) Toxic potential of materials at the nanolevel. Science 311:622–627
8. Fischer HC, Liu L, Pang KS, Chan WC (2006) Pharmacokinetics of nanoscale quantum dots: in vivo distribution, sequestration, and clearance in the rat. Adv Funct Mater 16:1299–1305
9. Lovric J, Cho SJ, Winnik FM, Maysinger D (2005) Unmodified cadmium telluride quantum dots induce reactive oxygen species formation leading to multiple organelle damage and cell death. Chem Biol 12:1227–1234
10. Choi AO, Cho SJ, Desbarats J, Lovric J, Maysinger D (2007) Quantum dot-induced cell death involves Fas upregulation and lipid peroxidation in human neuroblastoma cells. J Nanobiotechnology 5:1
11. Ryman-Rasmussen JP, Riviere JE, Monteiro-Riviere NA (2007) Surface coatings determine cytotoxicity and irritation potential of quantum dot nanoparticles in epidermal keratinocytes. J Invest Dermatol 127:143–153
12. Cho SJ, Maysinger D, Jain M, Roder B, Hackbarth S, Winnik FM (2007) long-term exposure to CdTe quantum dots causes functional impairments in live cells. Langmuir 23:1974–1980
13. Lovric J, Bazzi HS, Cuie Y, Fortin GR, Winnik FM, Maysinger D (2005) Differences in subcellular distribution and toxicity of green and red emitting CdTe quantum dots. J Mol Microbiol Biotechnol 83:377–385 (Berlin, Germany)
14. Shi H, Hudson LG, Liu KJ (2004) Oxidative stress and apoptosis in metal ion-induced carcinogenesis. Free radic Biol Med 37:582–593
15. Fasanya-Odewumi C, Latinwo LM, Ikediobi CO et al (1998) The genotoxicity and cytotoxicity of dermally-administered cadmium: effects of dermal cadmium administration. Int J Mol Med 1: 1001–1006
16. Sundaram N, Pahwa AK, Ard MD, Lin N, Perkins E, Bowles AP Jr (2000) Selenium causes growth inhibition and apoptosis in human brain tumor cell lines. J Neurooncol 46:125–133
17. Berthiaume M, Boufaied N, Moisan A, Gaudreau L (2006) High levels of oxidative stress globally inhibit gene transcription and histone acetylation. DNA Cell Biol 25:124–134
18. Strahl BD, Allis CD (2000) The language of covalent histone modifications. Nature 403:41–45
19. Callinan PA, Feinberg AP (2006) The emerging science of epigenomics. Hum Mol Genet 15 Spec No 1:R95–101
20. Esteller M (2006) The necessity of a human epigenome project. Carcinogenesis 27:1121–1125
21. Tsujimoto Y, Shimizu S (2005) Another way to die: autophagic programmed cell death. Cell death and differentiation 12(Suppl 2): 1528–1534
22. Funnell WR, Maysinger D (2006) Three-dimensional reconstruction of cell nuclei, internalized quantum dots and sites of lipid peroxidation. J Nanobiotechnology 4:10
23. Green M, Howman E (2005) Semiconductor quantum dots and free radical induced DNA nicking. Chem Commun (Camb) 7:121–123
24. Taghiyev AF, Guseva NV, Glover RA, Rokhlin OW, Cohen MB (2006) TSA-induced cell death in prostate cancer cell lines is caspase-2 dependent and involves the PIDDosome. Cancer Biol Ther 5:1199–1205
25. Gottlieb E, Tomlinson IP (2005) Mitochondrial tumour suppressors: a genetic and biochemical update. Nat Rev 5:857–866
26. McCord JM, Edeas MA (2005) SOD, oxidative stress and human pathologies: a brief history and a future vision. Biomed Pharmacother 59:139–142
27. Cheng WC, Berman SB, Ivanovska I et al (2006) Mitochondrial factors with dual roles in death and survival. Oncogene 25: 4697–4705
28. Culmsee C, Mattson MP (2005) p53 in neuronal apoptosis. Biochem Biophys Res Commun 331:761–777
29. Shibue T, Suzuki S, Okamoto H et al (2006) Differential contribution of Puma and Noxa in dual regulation of p53-mediated apoptotic pathways. EMBO J 25:4952–4962
30. Murphy ME, Leu JI, George DL (2004) p53 moves to mitochondria: a turn on the path to apoptosis. Cell cycle 3:836–839 (Georgetown, Tex)
31. Strom E, Sathe S, Komarov PG et al (2006) Small-molecule inhibitor of p53 binding to mitochondria protects mice from gamma radiation. Nat Chem Biol 2:474–479
32. Sawada M, Sun W, Hayes P, Leskov K, Boothman DA, Matsuyama S (2003) Ku70 suppresses the apoptotic translocation of Bax to mitochondria. Nat Cell Biol 5:320–329
33. Robertson RP, Harmon JS (2007) Pancreatic islet beta-cell and oxidative stress: The importance of glutathione peroxidase. FEBS Lett 581:3743–3748
34. Boix-Chornet M, Fraga MF, Villar-Garea A et al (2006) Release of hypoacetylated and trimethylated histone H4 is an epigenetic marker of early apoptosis. J Biol Chem 281:13540–13547
35. Grossman SR, Perez M, Kung AL et al (1998) p300/MDM2 complexes participate in MDM2-mediated p53 degradation. Mol Cell 2:405–415
36. Norbury CJ, Zhivotovsky B (2004) DNA damage-induced apoptosis. Oncogene 23:2797–2808